Decomposition of Multi-Exponential and Related Signals – Functional Filtering Approach

VAIRIS SHTRAUSS
Institute of Polymer Mechanics
University of Latvia
23 Aizkraukles Street, LV 1006 Riga
LATVIA
strauss@edi.lv

Abstract: - Decomposition of multi-exponential and related signals is generalized as an inverse filtering problem on a logarithmic time or frequency scale, and discrete-time filters operating with equally spaced data on a logarithmic scale (geometrically spaced on linear scale) are proposed for its implementation. Ideal prototypes, algorithms and types of filters are found for various time- and frequency-domain mono-components. It is disclosed that the ill-posedness in the decomposition originates as high sampling-rate dependent noise amplification coefficients arising from the large areas under the increasing frequency responses. A novel regularization method is developed based on the noise transformation regulation by filter bandwidth control, which is implemented by adaptation of the appropriate sampling rate. Algorithm design of decomposition filters is suggested joining together signal acquisition, regularization and discrete-time filter implementation. As an example, decomposition of a frequency-domain multi-component signal is considered by a designed filter.

Key-Words: - Decomposition, Multi-Component Signals, Distribution of Time Constants, Functional Filters, Logarithmic Sampling, Ill-posedness, Regularization

1 Introduction

Many areas of science and technology, such as material science, mechanics, biology, nuclear and electrical engineering, etc. face the problem of analysing monotonic and locally monotonic signals. The multi-component signals with the real decaying exponentials are probably the most studied case, although similar problems arise for many other monotonic mono-components, such as integrals, derivatives, real and imaginary parts of the Fourier transforms of the real exponentials, etc.

Although the problem of analysis of monotonic signals is not new, let remember the works [1-6] became already the classical ones, and is widely studied in various fields, and especially in relaxation spectroscopy [7-9], the problem remains a challenging signal processing task. The principal reasons are the exceedingly non-orthogonal behaviour of the monotonic signals no constituting an orthogonal base, and the fundamental ill-posedness in the sense that small perturbations in input signal can yield unrealistic high perturbations in the results of decomposition.

Motivation of this work is to analyze the problem from the up-to-date signal processing perspective [10] and to derive accurate, robust and computationally efficient algorithms.

2 Monotonic Multi-Component Signals

Multi-exponential decays are described by the following model

$$x(t) = \int_0^\infty g(\tau) \exp(-t/\tau) d\tau \,, \tag{1}$$

where $g(\tau)$ is a function of *distribution of time constants* (DTC) or *spectrum of time constants*. For the discrete (line) spectrum, $g(\tau)$ takes the form

$$g(\tau) = \sum_n g_n \delta(\tau - \tau_n) \,,$$

where $\delta(\tau)$ is the Dirac delta function.

In some fields, e.g. in relaxation studies [7-9], Eq. (1) is modified in the form

$$x(t) = \int_0^\infty f(\tau) \exp(-t/\tau) d\tau/\tau \,, \tag{2}$$

where new – so-called logarithmic DTC function $f(\tau) = g(\tau)\tau$ is introduced.

To generalize model (2) for other monotonic and locally monotonic signals, we modify it into the form

$$x(u) = \int_0^\infty f(\tau)K(u,\tau)d\tau/\tau, \quad (3)$$

where variable u is time or frequency, and kernel $K(u,\tau)$ represents a family of the time-domain and frequency-domain mono-components being of great importance in various fields

$$K(u,\tau) = \begin{cases} \exp(-u/\tau) & (4a) \\ \exp(-u/\tau)/\tau & (4b) \\ 1-\exp(-u/\tau) & (4c) \\ 1/(1+u^2\tau^2) & (4d) \\ u\tau/(1+u^2\tau^2) & (4e) \\ u^2\tau^2/(1+u^2\tau^2) & (4f) \end{cases}.$$

Kernel (4a) is the basic real decaying exponential, while (4b) and (4c) represent its derivative and integral, respectively. In its turn, kernels (4d) and (4e) embody the real and imaginary parts of the Fourier transform of kernel (4b). A pair of kernels (4f) and (4e) describes the frequency response of the system inverse to that characterized by a pair of kernels (4d) and (4e).

3 Decomposition Filters

3.1 Background

Since kernels (4a) – (4f) depend on the ratio or product of arguments u and τ, multi-component signal (3) may be converted in the form of the Mellin convolution type transform

$$x(u) = f(u) \overset{M}{*} k(u) = \int_0^\infty f(\tau)k(u/\tau)d\tau/\tau, \quad (5)$$

where $\overset{M}{*}$ denotes the Mellin convolution and $k(u/\tau)$ are kernels (4a) – (4f) modified in the form needed for converting Eq. (3) into Eq. (5) (so-called canonical kernels [11]).

In the spectral domain, convolution (5) is described as

$$X(j\mu) = F(j\mu)K(j\mu), \quad (6)$$

where $X(j\mu)$, $F(j\mu)$ and $K(j\mu)$ represent the Mellin transforms of appropriate functions $x(u)$, $f(u)$ and $k(u)$

$$X(j\mu) = \mathcal{M}[x(u); -j\mu] = \int_0^\infty x(u)u^{-j\mu-1}du.$$

The monotonic multi-component signals extend typically over long intervals of time or broad ranges of frequency [7-9], which is a reason for considering them on a logarithmic scale

$$u^* = \log_q u/u_0, \quad (7)$$

where u_0 is an arbitrary normalization constant. For logarithmic arguments (7), to remember that $u = u_0 q^{u^*}$, Eq. (5) alters into the appropriate Fourier convolution type transform ($u_0 = 1$)

$$x(q^{u^*}) = f(q^{u^*}) \overset{F}{*} k(q^{u^*}),$$

which also has spectral presentation (6), however, in this case, $X(j\mu)$, $F(j\mu)$ and $K(j\mu)$ represent the Fourier transforms of $x(q^{u^*})$, $f(q^{u^*})$ and $k(q^{u^*})$, i.e. functions with logarithmically transformed arguments. Thus, parameter μ, named the Mellin frequency [12], may be interpreted as a frequency of a signal (function), whose independent variable (time or frequency) is logarithmically transformed.

From (6) follows equation

$$F(j\mu) = X(j\mu)/K(j\mu) \quad (8)$$

describing DTC determination in the spectral domain. Equivalent representations of (8) in the time domain are the Mellin deconvolution

$$f(u) = x(u) \overset{M}{*} k^{-1}(u)$$

or the Fourier deconvolution

$$f(q^{u^*}) = x(q^{u^*}) \overset{F}{*} k^{-1}(q^{u^*}), \quad (9)$$

where $k^{-1}(u)$ and $k^{-1}(q^{u^*})$ are inverse kernels for linear and logarithmic arguments, respectively. The inverse kernels exist in the sense of generalized functions and the analytic expressions of $k^{-1}(u)$ and $k^{-1}(q^{u^*})$ for kernels (4a) – (4f) are not known. However, one according to (8) can derive the appropriate spectral counterparts of the inverse

kernels as the reciprocals of the Mellin or Fourier transforms of $k(u)$ or $k(q^{u^*})$

$$H(j\mu) = 1/\mathcal{M}[k(u); -j\mu] = 1/\mathcal{F}[k(q^{u^*}); -j\mu]. \quad (10)$$

Spectral representation (8) is a basis of the classical methods of Gardner [1], Schlesinger [2] and Roesler [3,4] implementing the decomposition by the following general scheme

$$f(\tau) = \mathrm{IDFT}\{\mathrm{DFT}[x(q^{u^*})]/\mathrm{DFT}[k(q^{u^*})]\}, \quad (11)$$

where IDFT and DFT are abbreviations of direct and inverse discrete Fourier transforms. Similarly, spectral representation (8) is used in the method Prost and Goutte [5,6] implementing the decomposition by the direct and inverse discrete Mellin transforms ((DMT) and (IDMT))

$$f(\tau) = \mathrm{IDMT}\{\mathrm{DMT}[x(u)]/\mathrm{DMT}[k(u)]\}. \quad (12)$$

On the other hand, deconvolution (9) may be considered as a *linear shift-invariant system* [10] or an *ideal decomposition filter* on a logarithmic time or frequency domain having impulse response $k^{-1}(q^{u^*})$ and frequency response $H(j\mu)$. Therefore, our idea is to implement deconvolution (9) in direct way by a discrete-time filter operating with equispaced samples on a logarithmic scale

$$f(u_m^*) = \sum_{n=-\infty}^{\infty} h[n]x(u_{m-n}^*), \quad (13)$$

where impulse response or a set of filter coefficients $h[n]$ represents a discrete-time version of kernel $k^{-1}(q^{u^*})$. In practice, of course, number of filter coefficients or filter length must be finite.

To take into consideration that equispaced samples on a logarithmic scale manifest as the logarithmically sampled data on linear scale where distance between samples increases according to the geometric progression

$$u_m^* = u_0\, q^m, \quad m = 0, \pm 1, \pm 2, \ldots,$$

algorithm (13) modifies into the following general form [11-13]:

$$f(u_0 q^m) = \sum_{n=-\infty}^{\infty} h[n]x\left(u_0 q^{m-n}\right). \quad (14)$$

Here, progression ratio q specifies the sampling rate in the sense that $\ln q$ plays formaly a role of sampling period on a logarithmic scale, whereas its reciprocal represents the appropriate sampling frequency.

Up to now, discrete-time filters [10] are used primarily for removing unwanted parts of a signal, such as random noise, or extracting useful parts of a signal, such as the components lying within a certain frequency range. Here, discrete-time filters with the logarithmic sampling perform a new function – carry out functional (integral) transformation of signals needed to implement decomposition (3). Due to this they have been named *functional filters* [11]. The specific target of the functional filters requires the design and application philosophy [11-15], which differs from that of conventional discrete-time filters.

The following general advantages may be listed [10] for the filtering approach:

(i) discrete-time filters have well-developed theory,
(ii) discrete-time filters are computationally efficient algorithms working without employing numerical integration,
(iii) they have uniform structure and implementation in software and hardware,
(iv) the problem solved by a discrete-time filter can be modified very easy by changing coefficients without modification of the common structure or implementation of the filter in hardware and software,
(v) correctly designed discrete-time filters have the guaranteed performance, such as accuracy and noise transformation, and no stability problems occur for them.

3.2 Algorithms of Decomposition Filters

Equation (3) with kernels (4a) and (4c) forms exactly the Mellin convolution type transform (5), for which algorithm (14) can be directly applied to. For kernel (4b), general algorithm (14) modifies into the form

$$f(u_0 q^m) = u_0 q^m \sum_{n=-\infty}^{\infty} h[n]x(u_0 q^{m-n}), \quad (15)$$

while for kernels (4d) – (4f), i.e. for the frequency-domain data, it modifies into the form

$$f(u_0 q^m) = \sum_{n=-\infty}^{\infty} h[n]x(q^{-m-n}/u_0). \quad (16)$$

Usually [11-13] the functional filters are used with the equal number of coefficients about their origins. Then, for odd number of filter coefficients N, general algorithm (14) takes the form

$$f(u_0 q^m) = \sum_{n=-(N-1)/2}^{(N-1)/2} h[n] x\left(u_0 q^{m-n}\right),$$

where the origin of impulse response coincides with zero sample $h[0]$. For even number of filter coefficients, the origin of impulse response may be located in the middle between the samples $h[-1]$ and $h[0]$, then algorithm (14) modifies into the form

$$f(u_0 q^m) = \sum_{n=-(N-2)/2-1}^{(N-2)/2} h[n] x\left(u_0 q^{m-0.5-n}\right). \quad (17)$$

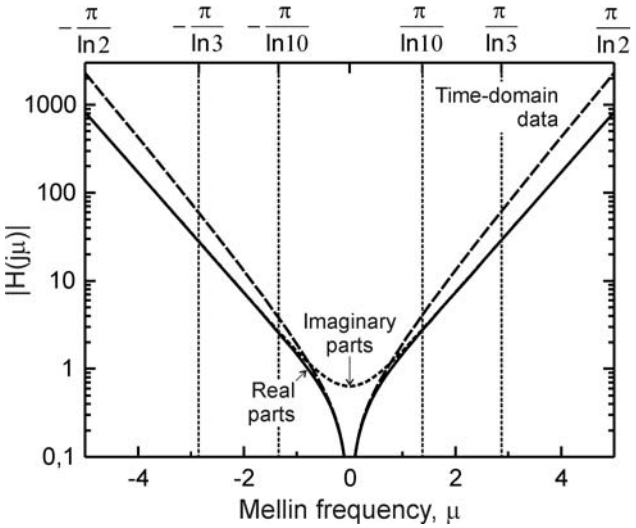

Fig. 1. Magnitude responses of three ideal decomposition filters. Vertical lines and upper X-axis show the bandwidths corresponding to different progression ratios q.

3.3 Types of Decomposition Filters

For six kernels (4a) – (4f), Eq. (10) gives the *three* following ideal frequency responses

$$H(j\mu) = \begin{cases} -1/\Gamma(-j\mu) & \text{for (4a) – (4c)} \quad (18a) \\ \pm j2\mathrm{sh}(\pi\mu)/\pi & \text{for (4d) and (4f)} \quad (18b) \\ 2\mathrm{ch}(\pi\mu)/\pi & \text{for (4e)} \quad (18c) \end{cases}$$

where (18a) relates to the time-domain data, (18b) – to the real parts, and (18c) – to the imaginary parts, respectively. Consequently, only *three independent* sets of coefficients $h[n]$ are necessary for implementing decomposition (3) for six kernels (4a) – (4f). Frequency responses (18a) – (18c) are similar – very fast growing functions (Fig. 1) indicating their inverse nature [11].

Frequency response (18a) of the ideal filter decomposing the time-domain data is a complex function. From the symmetry property of the Fourier transform [10], it follows that the appropriate impulse response has no symmetry, or, in other words, the filters recovering DTC from the time-domain data belong to so-called *non-linear phase systems*.

In contrast, frequency response (18b) is a pure imaginary function, while response (18c) is a real function. This indicates that the filters decomposing the frequency-domain data represent *linear phase systems* [10].

In Fig. 2(a, b), schematic approximation of ideal frequency response (18b) is shown by the appropriate frequency responses of a discrete-time filter

$$H\left(e^{j\mu}\right) = \sum_n h[n] \exp(-j\mu n \ln q) \quad (19)$$

with odd and even number of coefficients.

In the case of an odd number of coefficients, the decomposition filter represents *type III linear phase system* [10] having the frequency response, which crosses zero at the ends of bandwidth $\mu = \pm\pi/\ln q$ and at zero frequency (Fig. 2(a)). It has an anti-symmetric impulse response $h[n] = -h[-n]$ with $h[0] = 0$ (Fig. 2(c)). In the case of an even number of coefficients, the filter represents *type IV linear phase system* having the frequency response crossing zero at zero frequency and having non-zero values at the ends of the bandwidth $\mu = \pm\pi/\ln q$ (Fig. 2(b)) with an anti-symmetric impulse response $h[n] = -h[-n-1]$ (Fig. 2(d)).

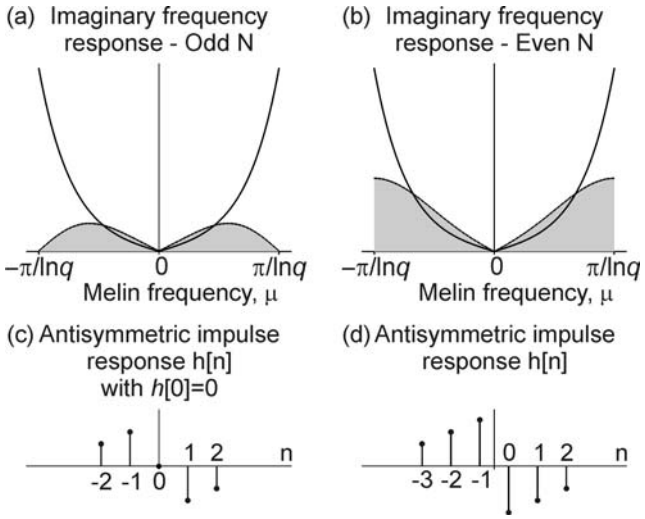

Fig. 2. Schematic approximation of frequency response (18b) with an odd (a) and an even (b) number of filter coefficients, and examples of the appropriate discrete impulse responses (c) and (d).

In Fig. 3, the similar plots are shown for the filter with frequency response (18c) decomposing the imaginary parts. In this case, the filter with an odd number of coefficients represents *type I linear phase system* with a symmetric impulse response $h[n] = h[-n]$ (Fig. 3(c)), while the filter with an even number of coefficients represents *type II linear phase system* with the following symmetric impulse response $h[n] = -h[-n-1]$ (Fig. 3(d)).

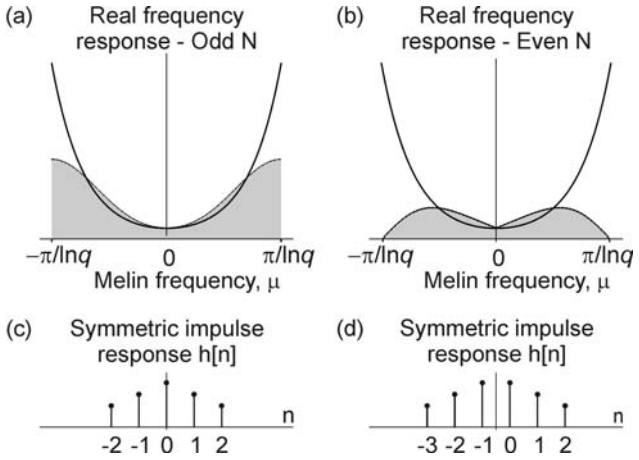

Fig. 3. Schematic approximation of frequency response (18c) with odd (a) and even (b) number of filter coefficients, and examples of the appropriate discrete impulse responses (c) and (d).

4 Ill-posedness, sampling rate and noise transformation

The noise behaviour of a decomposition filter may be characterized by *noise coefficient S* transforming input noise variance σ_x^2 into the output noise variance σ_y^2

$$\sigma_y^2 = S\sigma_x^2$$

being equal to sum of the square filter coefficients

$$S = \sum_{n=1}^{N} h^2[n]. \qquad (20)$$

The Parseval theorem [10] allows determining noise coefficient *S* also through frequency response

$$S = \ln q/(2\pi) \int_{-\pi/\ln q}^{\pi/\ln q} \left|H(.)\right|^2 d\mu, \qquad (21)$$

where ideal frequency responses (18a) – (18c) give inherent to the decomposition theoretical noise coefficients S_{theor}, while frequency response (19) of a discrete-time filter provides actual experimental noise coefficient (20) for the given progression ratio.

As it follows from Eq. (21), increasing the sampling rate (decreasing q) extends bandwidth $[-\pi/\ln q, \pi/\ln q]$ of a filter (see Fig. 1), and, consequently, the appropriate squared area under the frequency response quoting the value of the noise coefficient. Due to the increasing frequency responses the theoretical noise coefficient S_{theor} increases with decreasing progression ratio q and tends to ∞, when q approaches 1 (Fig. 4). Thus, the ill-posedness of the decomposition manifests as the large noise amplification coefficient coming from the large area under the frequency response, which, in its turn, results from the wide bandwidth. Several useful conclusions may be drawn from the above that degree of the ill-posedness:

(i) may be related to and characterized quantitatively by the noise coefficient,
(ii) depends strongly on the sampling rate and arises only at small progression ratios q (fast sampling rates), and
(iii) may be controlled or the decomposition may be regularized by choosing the appropriate sampling rate, which through establishing the bandwidth regulates its noise transformation coefficient.

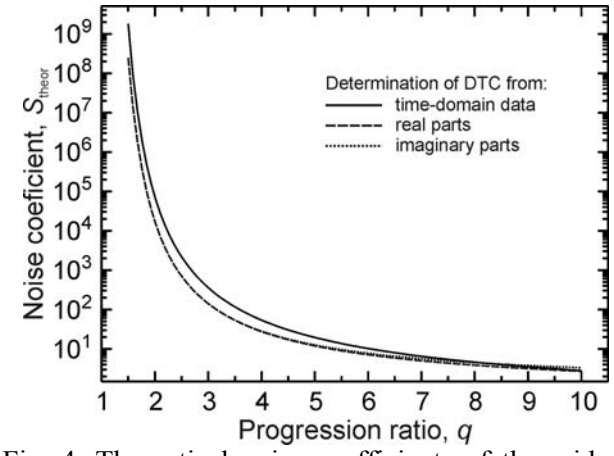

Fig. 4. Theoretical noise coefficients of three ideal inverse filters (18a) – (18c).

The last conclusion substantiates an alternative to the traditional regularization strategies based on reducing the sensitivity to measurement errors by limiting the areas under the frequency responses "vertically" (Fig. 5(a)) by suppressing them, for example, by adding special functional $\alpha(\mu)$ in reciprocating frequency response (10)

$$H_\alpha(j\mu) = 1/\{\ \mathcal{M}[k(u); -j\mu] + \alpha(\mu)\},$$

which distorts the shape of the frequency response of an inverse filter, but achieves that $\lim_{\mu\to\pm\infty}\left|H_\alpha(j\mu)\right| = \alpha^{-1}(\infty) \neq \infty$ and, so limits the noise coefficient.

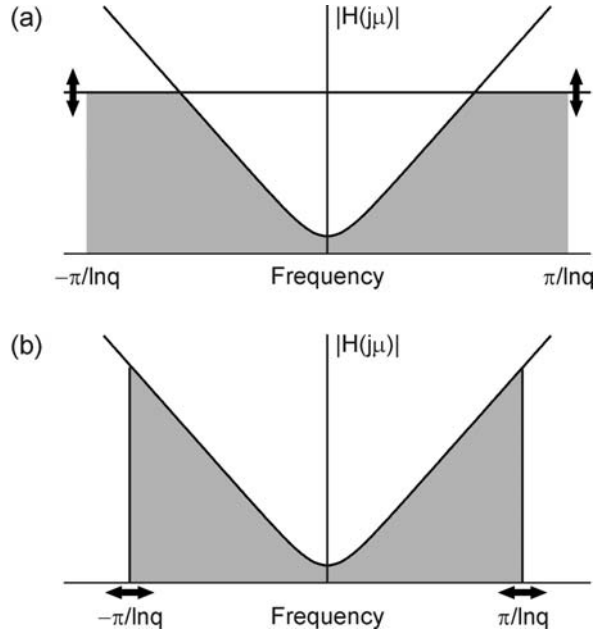

Fig. 5. Regularization methods based on limiting frequency response (a) and bandwidth control (b). Arrows show the direction of variation of area (shaded) under the frequency response.

We propose to limit the areas under the frequency responses "horizontally" (Fig. 5(b)) – by controlling the bandwidths of filters by choosing the appropriate value of q, i.e. by employing a natural – *inherent regularization capability of a linear discrete-time algorithm* []. The proposed approach has two advantages: (i) it does not distort the shape of frequency response, and, therefore, promises eventually the higher accuracy; and (ii), as it will be shown further in the next Section, the approach allows to determine explicitly regularization parameter q and to relate it to the specification of an algorithm, while there no strong criterion for determination of regularization parameters for the traditional regularization methods limiting the frequency responses "vertically".

5 Algorithm Design

The conventional two-step signal processing approach [10] consisting of separate (i) discrete signal acquisition step, where the signal is sampled uniformly above its Nyquist rate, and (ii) discrete-time algorithm implementation step, is not applicable. In the decomposition, on the one hand, choice of the sampling rate (signal acquisition) melds with the regularization because the needed noise immunity must be ensured. On the other hand, the filter length (implementation of algorithm) cannot be chosen free because possible combinations of q and N are limited by the time or frequency ranges of the available input data.

Thus, algorithm design of the decomposition filters is a complex problem, which must integrate together signal acquisition, regularization and discrete-time algorithm implementation steps and, additionally, take into account the time or frequency ranges of the available input data. To link q and N with the input data, a parameter – dynamic range of time or frequency of input signal portion used for computing an output sample (further 'input window range')

$$d_x = u_+ / u_- = q^{N-1}, \tag{22}$$

is introduced, which determines the combinations of q and N allowable for the filter design.

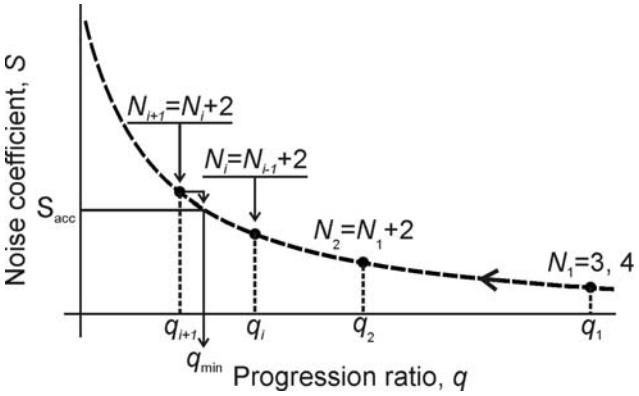

Fig. 6. Finding a combination of progression ratio q and number of filter coefficients N for the regularization based on filter bandwidth control.

The appropriate algorithm design method is described in [14]. The procedure is based on the typical decrease of noise coefficient S with progression ratio q (see Fig. 4). Trial filters are designed for the combinations of q and N allowed by Eq. (22) starting with one operating at explicitly large q_1 corresponding to small number of coefficients (normally $N_1 = 3 \text{ or } 4$) and giving low noise coefficient $S < S_{acc}$ (Fig. 6) by subsequent iterative increase of number of coefficients $N_{i+1} = N_i + 2$ and the appropriate decrease of q. When S_{acc} is exceeded the iterative process is

terminated. After that the final values of $q \approx q_{\min}$ and, may be d_x are specified.

For the stated q and N, the decomposition filters are designed by the identification method [11] where a pair of theoretical functions interrelated with each other by transform (3) is used as input and output signals in the filter design. An advantage of the identification method executing the time-domain optimization is that it effectively disposes of various secondary effects such as data truncation, rounding-off, etc. and allows designing filters of various types (e.g. with linear and non-linear phase).

6 Example of Decomposition Filter

Below, as an example, type IV linear phase functional filter (even N) will be considered for decomposition of frequency-domain multi-component signals with mono-components (4d) and (4f), which must ensure noise coefficient $S < 10$ and employ input window range $d_x < 500$ [16,17].

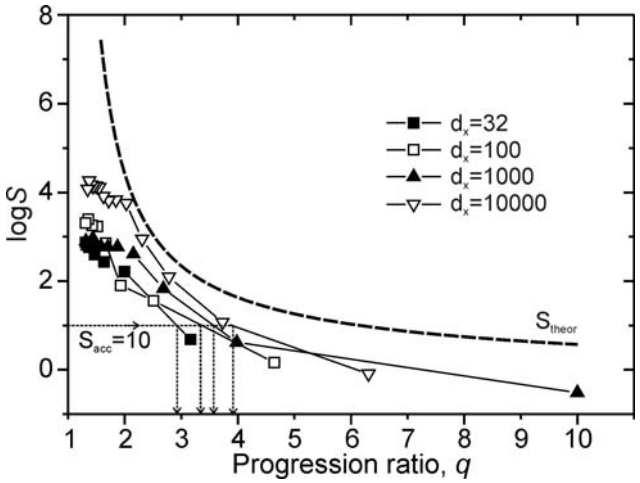

Fig. 7. Theoretical and experimental noise coefficients of decomposition filters having even number of coefficients for various input window ranges d_x. Horizontal and vertical arrows show the values of S and q corresponding to acceptable noise coefficient $S_{acc} = 10$.

To estimate the relationship between sampling rate and noise transformation, the functional filters have been designed by the identification method and their noise coefficients have been investigated for the combinations of q and N allowed by a selected set of input window ranges d_x (32, 100, 1000, 10000) covering fairly fully the relevant cases for practice. The obtained results are shown in Fig. 7, where noise coefficient S is shown as a function of progression ratio q for the examined cases. As it is seen, the identification method gives filters having the noise coefficients, which are lower than theoretical ones. To ensure noise coefficient $S_{acc} \approx 10$ progression ratio must be within the interval $q = 2.9...3.9$. We choose q = 3.3. Then $N = 6$ according to (22) gives $d_x = 391 < 500$. By the identification method, the following coefficients have been obtained [16-18]:

$$h[6] = \{-0.033296, 0.129207, -1.05880, \\ 1.05880, -0.129207, 0.033296\}. \quad (23)$$

According to (20) the designed filter has noise coefficient S = 2.28, which means that the noise variance for recovered DTC is amplified 2.28 times or the standard deviation of DTC noise is amplified $\sqrt{2.28} = 1.51$ times to compare with that of the input signal.

In Fig. 8, some examples of DTCs are shown for discrete spectra recovered from noiseless input data by filter (23). DTCs are calculated by algorithm (16) modified by introducing substitution $\tau = u_0 q^m$ and summation according to (17) into the form

$$f(\tau) = \sum_{n=-3}^{2} h[n] x(3.3^{-0.5-n} / \tau).$$

Notice that the designed filter gives DTCs without non-physical oscillations. However, such smooth spectra and relatively high noise immunity are achieved at the expense of decreased resolution; the filter allows separating two spectral lines only, if $\tau_{i+1} / \tau_i < 0.2$ or $\tau_{i+1} / \tau_i > 5$.

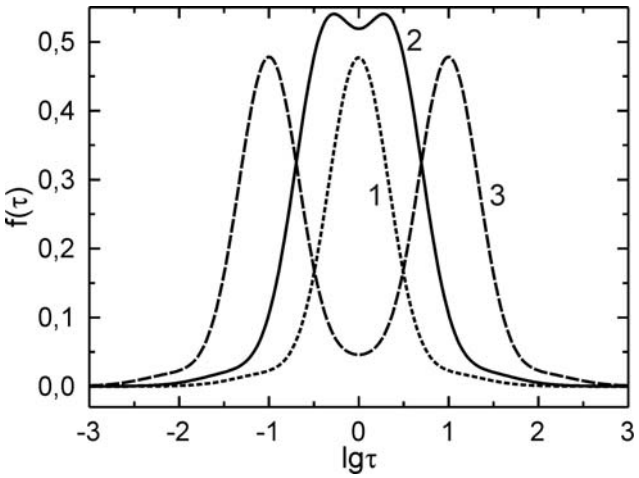

Fig. 8. Recovered discrete DTCs from the noiseless input data: unity spectrum at $\tau = 1$ (curve 1); two unity line spectra at $\tau_1 = 0.42$ and $\tau_2 = 2.37$ (curve 2) and at $\tau_1 = 0.1$ and $\tau_2 = 10$ (curve 3).

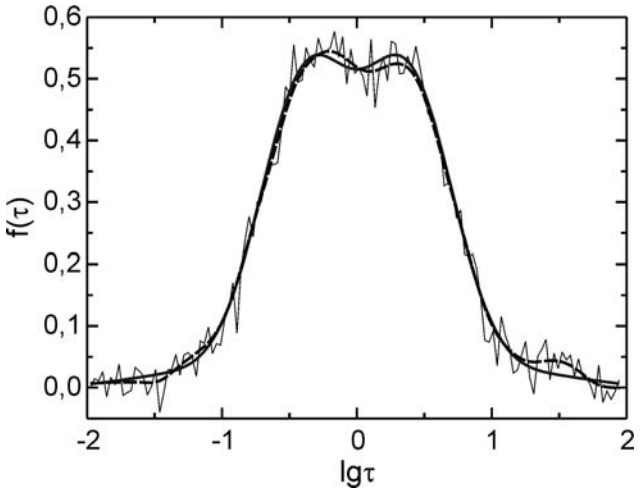

Fig. 9. DTCs for two unity line spectra at $\tau_1 = 0.42$ and $\tau_2 = 2.37$ recovered from the noiseless input signal (fat solid curve) and noisy input signal (24) with $e = 0.05$ (thin solid curve) and smoothed DTC (dotted curve).

In Fig. 9, DTCs are compared recovered from the noiseless input signal and from the noisy signal corrupted by additive random noise

$$x_{noisy}(u_m) = x_{exact}(u_m) + e \cdot n(m), \qquad (24)$$

where $n(m)$ is the pseudorandom sequence within interval [-1,1] with zero mean having the Gaussian probability distribution, and e is a factor specifying amplitude of the input noise. The simulation results confirm the above mentioned noise amplification. Thus, the recovered DTC from the noisy data (thin solid curve) indeed represents DTC obtained from the noiseless data (fat solid curve) with additive noise component $\sqrt{S} \cdot e \cdot n(m) \approx 0.076 \cdot n(m)$. The simulations show that the noise component can be effectively reduced by smoothing. The noisy DTC smoothed by simple 5-point averaging

$$f(\tau_m) = \frac{1}{5}\sum_{n=-2}^{2} f(\tau_{m+n})$$

gives the result (dotted curve), which is in rather good agreement with DTC obtained from the noiseless input data.

7 Why Decomposition Filters Work?

Despite that the spectral methods (11) and (12), and the decomposition filters are mathematically equivalent techniques, the latter approach has some advantages. First, its realization with hardware or software is simpler, in particular, to take into account the short impulse responses.

Second, the proposed filtering approach integrating together signal acquisition, regularization and discrete-time algorithm implementation ensures superior performance over spectral approaches (11) and (12) in terms of accuracy and noise immunity.

The Mellin or Fourier transform of the noisy signals to be limited by a finite length window contributing the basic errors in the spectral approaches is not performed. Instead, the filters operating with optimal sampling rate securing the desired noise immunity and number of coefficients allowed by the available input data are designed by time-domain optimization [11] ensuring maximum accuracy of the recovered DTC.

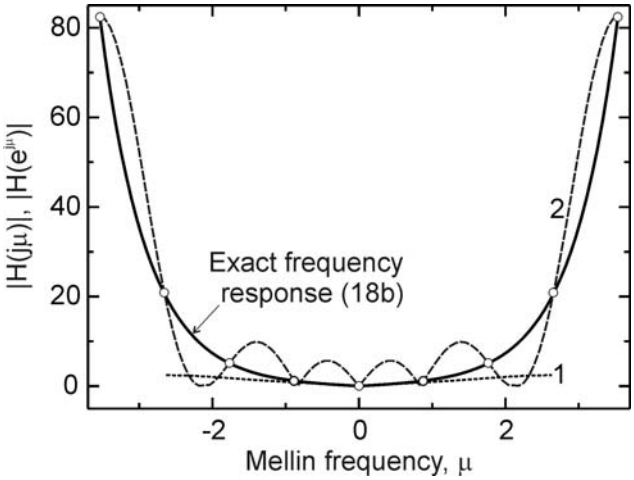

Fig. 10. Actual frequency response of filter (23) (curve 1) and reciprocal $1/\mathrm{DFT}[k(q^{u^*})]$ for $N = 8$ and $d_x = 500$ (curve 2).

In Fig. 10, actual frequency response $H(e^{j\mu})$ of filter (23) and schematic formation of equivalent reciprocal $1/\mathrm{DFT}[k(q^{u^*})]$ for approach (11) are shown. As seen, the actual frequency response calculated by (19) from the coefficients obtained by time-domain optimization is a smooth curve, which, except the region around zero frequency, fits very poor the exact frequency response (18b). Nevertheless, filter (23) has the high performance in terms of accuracy and noise immunity. In the same time, DFT produces the exact frequency response at the points defined by N (circles) with wild fluctuations between the points. As a result, the accuracy of DTC recovery for the spectral approach is considerable smaller, while the sensitive to noise or the degree of ill-posedness is incredibly larger.

7 Conclusions

Discrete-time filters operating with equally spaced data on a logarithmic time or frequency scale (geometrically spaced on linear scale) are proposed for decomposition of multi-exponential and related signals, such as integrals, derivatives, real and imaginary parts of the Fourier transforms of the real exponentials. It is established that the decomposition for a variety of mono-components reduces to the three inverse filters, i.e. for the time-domain mono-components, for the real and the imaginary parts of frequency-domain mono-components, respectively. The appropriate filter algorithms are derived. It is disclosed that decomposition of the time-domain mono-components requires non-linear phase filters, while linear phase filters are necessary for decomposition of frequency-domain mono-components, namely type I and II linear phase filters are needed for the imaginary mono-components and type III and VI linear phase filters – for real mono-components.

It is demonstrated that the ill-posedness in the decomposition manifests as high sampling-rate dependent noise amplification coefficients arising from the large areas under the increasing frequency responses of the inverse decomposition filters. A novel regularization method allowing to determine explicitly the value of the regularization parameter is developed based on noise transformation regulation by filter bandwidth control implemented by adaptation of the appropriate sampling rate. Algorithm design of the decomposition filters is suggested integrating together the signal acquisition, the regularization and the discrete-time filter implementation. As an example, decomposition of a frequency-domain multi-component signal is considered by a designed filter.

References:

[1] D.G. Gardner J.C. Gardner, G. Laush and W.W. Meinke, Method for analysis of multicomponent exponential decay curves, *J. Chem. Phys.*, Vol. 31, No. 4, 1959, pp. 978-986.

[2] T. Schlesinger, Fit to experimental data with exponential functions using the fast Fourier transform, *Nucl. Instr. Meth.*, Vol. 106, No. 3, 1973, pp. 503-508.

[3] F.C. Roesler and J.R.A. Pearson, Determination of relaxation spectra from damping measurements, *Proc. Phys. Soc*., Vol. 67, No. 412B, 1954, pp. 338-347.

[4] F.C. Roesler, Some applications of Fourier series in the numerical treatment of linear behaviour, *Proc. Phys. Soc.*, Vol. 68, No. 422B, 1955, pp. 89-96.

[5] R. Prost and R. Goutte, Linear systems identification by Mellin deconvolution, *Int. J. Control*, Vol. 23, No. 4, 1976, pp. 713-720.

[6] R. Prost and R. Goutte, Performance of the method of linear systems identifications by Mellin deconvolution, *Int. J. Control*, Vol. 25, No. 1, 1977, pp. 39-51.

[7] J.D. Ferry, *Viscoelastic Properties of Polymers*, 3rd. ed., J. Wiley and Sons, 1980.

[8] N.G. McCrum, B.E. Read, G. Wiliams, *Anelastic and Dielectric Effects in Polymer Solids*, J. Wiley and Sons, 1967.

[9] A.K. Jonscher, *Dielectric Relaxation in Solids*, Chelsea Dielectric, 1983.

[10] A. V. Oppenheim, R. V. Schafer, *Discrete-Time Signal Processing*, Sec. Ed., Prentice-Hall International, 1999.

[11] V. Shtrauss, Functional conversion of signals in the study of relaxation phenomena, *Signal Processing*, Vol. 45, 1995, pp. 293-312.

[12] V. Shtrauss, Digital signal processing for relaxation data conversion, *J. Non-Crystal. Solids*, Vol. 351, 2005, pp. 2911-2916.

[13] V. Shtrauss, Signal processing in relaxation experiments, *Mech. Comp. Mat.*, Vol. 38, 2002, pp. 73-88.

[14] V. Shtrauss, Sampling and algorithm design for relaxation data conversion, *WSEAS Transactions on Signal Processing*, Vol. 2, Issue 7, 2006, pp. 984-990.

[15] V. Shtrauss, Sampling in relaxation data conversion, *Proc. 10th WSEAS International Conference on SYSTEMS*, Vouliagmeni, Athens, Greece, July 10-12, 2006, pp. 37-42.

[16] V. Shtrauss, Inverse filters for decomposition of multi-exponential and related signals, *Proc. 7th WSEAS International Conference on Systems Theory and Scientific Computation (ISTASC'07)*, Vouliagmeni, Athens, Greece, August 24-26, 2007, pp.135-140.

[17] V. Shtrauss, Decomposition filters for multi-exponential and related signals, *International journal of Mathematical Models and Methods in Applied Sciences*, Vol. 1, Issue 3, 2007, pp. 137-142.

[18] V. Shtrauss, Digital estimators of relaxation spectra, *J. Non-Crystal. Solids*, Vol. 353, 2007, pp. 4581-4585.